Ruthenium polypyridine complexes as sensitizers in NiO based p-type dye-sensitized solar cells: Effects of the anchoring groups

Yann Pellegrin[a], Loïc Le Pleux[a], Errol Blart[a], Adèle Renaud[a], Benoit Chavillon[b], Nadine Szuwarski[a], Mohammed Boujtita[a], Laurent Cario[b], Stéphane Jobic[b], Denis Jacquemin[a,**], Fabrice Odobel[a,*]

[a] CEISAM, Université de Nantes, CNRS, 2 rue de la Houssinière, 44322 Nantes Cedex 3, France
[b] Institut des Matériaux Jean Rouxel, Université de Nantes, CNRS, 2 rue de la Houssinière, 44322 Nantes Cedex 3, France

ARTICLE INFO

ABSTRACT

In this contribution, we investigate the photovoltaic performances of four ruthenium trisbipyridine complexes in NiO based dye-sensitized solar cells (DSSC). The four complexes differ by the nature of the anchoring groups, which are either carboxylic acids, biscarbodithioic acids catechol or methyl phosphonic acids. The properties of the dyes were studied by electrochemistry, absorption and emission spectroscopies, surface binding measurements, time-dependent density functional theory (TDDFT) as well as by determining their photoconversion efficiencies in DSSCs under AM 1.5. We show that these simple dyes are relatively efficient sensitizers in NiO-based DSSCs, since some of them give photoconversion efficiencies comparable to that of a standard benchmark dye coumarin **C343**. We also demonstrate that both catechol and methyl phosphonic acid are promising binding groups for NiO sensitizers to replace classical carboxylic acids in NiO sensitizers and finally we report molecular design rules to elaborate a new generation of better performing ruthenium polypyridine sensitizers.

© 2011 Elsevier B.V. All rights reserved.

1. Introduction

There is currently a growing interest in the development of dye-sensitized solar cells (DSSCs) based on p-type inorganic semiconductors (p-SCs) such as nickel oxide [1]. This new type of solar cell is based on the hole injection in the valence band of the p-SC from the photoexcited sensitizer. Accordingly, the specific electronic properties of the ideal sensitizer for p-SCs significantly differ from those designed for classical Grätzel cells based on the sensitization of a n-type semiconductor (n-SC) such as titanium dioxide. In the latter case, the dye must be a strong reducer in its excited-state to inject an electron in the conduction band of the n-SC. Actually, the electronic requirements of the sensitizers for p-SCs are just the opposite of those for n-SC. In addition, the sensitizers must be functionalized with anchoring groups, first to firmly graft them on the semiconductor surface and second to provide a significant electronic coupling with the semiconductor wavefunction in order to ensure an efficient charge tunnelling from the sensitizer excited-state into the semiconductor [2–5]. For hole injection into a p-SC, this parameter is optimized when the highest occupied molecular

orbital (HOMO) of the dye significantly extends on the anchoring groups in order to overlap with the valence band (VB) orbitals of the semiconductor. Let us notice that the majority of dyes tested with p-type semiconductors were immobilized through carboxylic acid groups [1], which is not necessarily optimal for hole injection, since they generally bear large densities of the lowest unoccupied molecular orbital (LUMO) rather than of the HOMO [2–5]. For an efficient hole injection into the VB of a p-SC, a vectorial electron shift from the anchoring group towards the extremity of the dye is sought. As a result, electron withdrawing anchoring groups do not fulfil this requirement and would rather lead to a situation where positive charge density is moved in an unfavourable direction to assist the hole injection and to prevent the charge back recombination. Besides, with a view of performing charge photoinjection reactions, charge transfer excited-states such as those found in polypyridine ruthenium complexes are particularly relevant. Indeed, polypyridine ruthenium complexes perform particularly well as sensitizers in classical Grätzel DSSCs [6–8] and more generally as dyes in molecular devices for solar energy conversion [9,10]. In addition, the strong reducing potential of these complexes makes this class of compounds particularly appealing in view of performing photocatalytic processes with such photocathodes [11–15]. Surprisingly, synthetic ruthenium polypyridine complexes were never tested in p-type DSSCs.

In this paper, we report: (1) the electrochemical and the photophysical properties; (2) the surface binding properties; (3)

* Corresponding author. Tel.: +33 251125429; fax: +33 251125402.
** Corresponding author. Tel.: +33 251125564; fax: +33 251125402.
E-mail addresses: Denis.Jacquemin@univ-nantes.fr (D. Jacquemin),
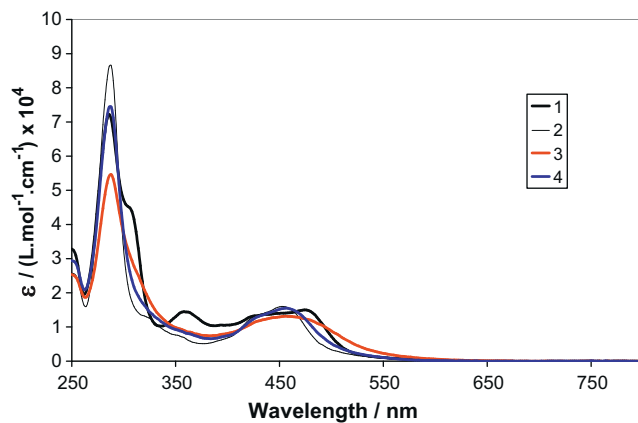Fabrice.Odobel@univ-nantes.fr (F. Odobel).

Chart 1. Structures of the ruthenium complexes investigated in this work.

time-dependent density functional theory (TDDFT) simulations; and (4) the photoconversion efficiencies in p-DSSC of a series of four ruthenium(II) trisbipyridyl complexes functionalized with different anchoring groups (Chart 1). The compounds synthesized herein enable not only to test the suitability of ruthenium polypyridine complexes as sensitizers in p-DSSCs but also to explore the pertinence of using other anchoring groups than the classical carboxylic acid group, which is the sole binding group used for NiO DSSCs up to now. These complexes were not prepared to break any photovoltaic records, since it was anticipated that they would display the classical orange colour with a relatively modest extinction coefficient, preventing thus to reach high performances. Similar trisbipyridine ruthenium complexes were also reported to be modest sensitizers in classical TiO$_2$ based Grätzel cells due to low LHE (Light Harvesting Efficiency) [16,17]. The results of this study firstly demonstrate that both catechol and methyl phosphonic acid are promising binding groups for NiO sensitizers to replace classical carboxylic acids in NiO sensitizers and secondly that through a rational ligand design, it is possible to achieve efficient sensitization of p-type semiconductors with ruthenium polypyridine complexes.

1.1. Materials and general synthetic procedures

Chemicals were purchased from Aldrich, Acros or ABCR and used as received. Air sensitive reactions were carried out under argon in dry solvents and glassware. Thin-layer chromatography (TLC) was performed on aluminium sheets precoated with Merck 5735 Kieselgel 60F254. Column chromatography was carried out either with Merck 5735 Kieselgel 60F (0.040–0.063 mm mesh) or with SDS neutral alumina (0.05–0.2 mm mesh). [Ru(bpy)$_2$(4,4′-biscarboxy-2,2′-bipyridine)](PF$_6$)$_2$ **1** [18], [Ru(bpy)$_2$(4,4′-(CH$_2$PO$_3$H$_2$)$_2$bpy)](PF$_6$)$_2$ **2** [17], complex **4** [19] and *cis*-Ru(bpy)$_2$Cl$_2$·2H$_2$O [20] were prepared according to literature methods. Complex Ru(bpy)$_2$(4,4′-biscarbodithioic acid-2,2′-bipyridine)](PF$_6$)$_2$ **3** was prepared by oxidation of the known 4,4′-bis(chloromethyl)-2,2′-bipyridine]bis[2,2′-bipyridine] ruthenium dichloride [21] by elemental sulphur as described below.

1.1.1. [Ru(bpy)$_2$(bpy(CS$_2$H)$_2$)](PF$_6$)$_2$ **(3)**

Elemental sulphur (4 equiv., 69 mg) and sodium methanolate (4 equiv., 116 mg, 2.1 mmol) were placed in anhydrous methanol (50 mL) under argon atmosphere and refluxed until the sulphur was completely dissolved (ca. 2 h). Then [Ru(bpy)$_2$(4,4′-(CH$_2$Cl)$_2$bpy)](PF$_6$)$_2$ (1 equiv., 512 mg, 0.54 mmol) was added in the solid form to the reaction mixture, which was refluxed overnight. The solvent was evaporated and the obtained red solid was dissolved in water. Acidification with diluted aqueous hydrochloric

acid led to the precipitation of the complex, which was filtered off and washed several times with water. The product was dissolved in a minimum amount of acetonitrile. Addition of a saturated aqueous solution of NH$_4$PF$_6$ led to the precipitation of **3** (465 mg; 86%) as a dark orange solid, which was collected by filtration, washed with H$_2$O and dried under vacuum. ^{1}H NMR (300 MHz, CD$_3$CN): δ 8.49 (m, 6H), 8.05 (m, 6H), 7.72 (m, 4H), 7.39 (m, 6H). Anal. Calcd for C$_{36}$H$_{35}$F$_{12}$N$_7$O$_2$P$_2$RuS$_4$ (**1** + 2 MeOH and 1 CH$_3$CN): C, 38.7; H 3.2; N, 8.7; S 11.5. Found: C, 38.5; H, 2.8; N, 8.4; S 11.3.

1.2. Analytical measurements

^{1}H and ^{13}C NMR spectra were recorded on a Bruker ARX 300 MHz. Chemical shifts for ^{1}H NMR spectra are referenced relative to residual protium in the deuterated solvent (CDCl$_3$ δ = 7.26 ppm for ^{1}H and δ = 77.16 ppm for ^{13}C). MALDI-TOF analyses were performed on a Bruker Ultraflex III, microTOF Q spectrometer in positive linear mode at 20 kV acceleration voltage with 2,5-dihydroxybenzoic acid (DHB) or dithranol as matrix. Electrochemical measurements were performed with a potentiostat-galvanostat AutoLab controlled by resident GPES software (General Purpose Electrochemical System 4.9) using a conventional single-compartment three-electrode cell. The working electrode was a Pt electrode, the auxiliary was a Pt wire of 10 mm long and the reference electrode was the saturated potassium chloride calomel electrode (SCE). The supported electrolyte was 0.1 N Bu$_4$NPF$_6$ in DMF and the solutions were purged with argon before the measurements. All potentials are quoted relative to SCE. In all the experiments the scan rate was 100 mV/s. UV–visible absorption spectra were recorded on a UV-2401PC Shimadzu spectrophotometer. Fluorescence spectra were recorded on a SPEX Fluoromax fluorimeter.

1.3. Preparation of dye-sensitized nanocrystalline NiO electrodes

Conductive glass substrates (F-doped SnO$_2$) were purchased from Pilkington (TEC8, sheet resistance 8 Ω/square). Conductive glass substrates were successively cleaned by sonication in soapy water, then ethanol for 10 minutes before being fired at 450 °C for 30 min. Once cooled down to room temperature, FTO plates were rinsed with ethanol and dried in ambient air. NiO films were prepared in two steps. A first layer of NiO (Nickel oxide nanopowder, Inframat Advanced Materials) was screen printed and annealed at 550 °C for 10 min; second, a layer of F108-templated precursor solution was doctor bladed onto the screen printed NiO, followed by sintering at 450 °C for 30 min

(thickness was measured by a Sloan Dektak 3 profilometer) according to literature procedures [22,23]. The prepared NiO electrodes were soaked while still hot (100 °C) in a 0.25 mM solution of each ruthenium complex in tertbutanol/acetonitrile 1:1 (unless otherwise mentioned) overnight in the dark at room temperature.

1.4. Dye-sensitized solar cell fabrication

Sealed sandwich cells were prepared using the dye-sensitized electrodes as the working electrodes and platinum-coated conducting glass electrodes as counter electrodes. The latter were prepared by chemical deposition of platinum from hexachloroplatinic acid in distilled isopropanol (2 mg per mL). The two electrodes were placed on top of each other using a thin transparent film of Surlyn polymer (DuPont, 25 μm) as a spacer to form the electrolyte space. The empty cell was tightly held, and the edges were heated to 130 °C to seal the two electrodes together. A drop of electrolyte consisting of 1.0 M LiI and 0.1 M I_2 in acetonitrile was introduced through a predrilled hole in the counter electrode by vacuum backfilling, and was sealed afterward. The cell had an active area of ca. 0.25 cm^2.

1.5. Photoelectrochemical measurements

The current–voltage characteristics were determined by applying an external potential bias to the cell and measuring the photocurrent using a Keithley model 2400 digital source meter. The overall conversion efficiency η of the photovoltaic cell is calculated from the integral photocurrent density (J_{sc}), the open-circuit photovoltage (V_{oc}), the fill factor of the cell (ff), and the intensity of the incident light (I_{Ph})

1.6. Binding constant measurements

In these experiments, 8.1 ± 0.05 mg of NiO nanoparticles (Nickel oxide nanopowder, Inframat Advanced Materials) were immersed in several acetonitrile solutions of complexes 1–4 for one week at 20 °C (the concentrations were set between 0.2 and 1.2 mmol L^{-1}, and assessed by spectrophotometry, using the extinction coefficients indicated in Table 1). The NiO particles were subsequently removed by filtration and the supernatant was subjected to spectrophotometry analysis in order to determine the concentration of the solution of the adsorbate at the equilibrium (C_{eq}). The amount of adsorbed dyes (n_{occ}) was calculated from the difference in the optical density prior and after equilibration with the NiO. Then, the data were plotted according to the Langmuir isotherm equation (Eq. (1)):

$$\frac{C_{eq}}{n_{occ}} = aC_{eq} + b \qquad (1)$$

The slope $a = 1/n_{max}$ is the reciprocal amount of adsorbate at monolayer coverage and the association constant (K) is calculated as $K = a/b$.

The concentration at monolayer coverage (Γ_{max}) was calculated by dividing n_{max} by the surface area of the NiO (120 m^2/g). The latter

value was given by the supplier (Inframat) and was confirmed by a BET analysis.

1.7. Computational methods

All quantum mechanical simulations have been performed with the Gaussian09 program [24]. A well-established three-step procedure has been used [25]: (1) the ground-state geometries of all compounds have been determined with the PBE0 functional [26] through a force-minimization process. The first triplet states have also been optimized similarly (see Supporting Information). The optimizations have been considered converged when the residual mean square force passed below the 1×10^{-5} au threshold (tight threshold in Gaussian); (2) the vibrational spectrum of each derivatives has been determined analytically at the same level of theory and it has been checked that all structures correspond to true minima of the potential energy surface; (3) the first thirty singlet and first ten triplet low-lying excited-states have been determined within the vertical TD-DFT using the ground-state geometry. Several basis sets have been tested (see SI) and it turned out that using 6-31G(d) for ground-state properties and 6–31 + G(d) for excited-state properties yields converged transition energies. For Ru, we have selected the CEP-121G basis set (and pseudopotential), augmented with a p diffuse function ($\alpha = 0.08$) during the TD-DFT calculation. Such choice has been previously advocated for similar studies [27]. The TD calculations used the same PBE0 functional, test calculations performed with the range-separated CAM-B3LYP [28] provided similar shapes but less accurate transition energies (see SI). It is well-known that solvent effects play a major role in DSSC [27–29] and they have been accounted for by means of the Conducting Polarizable Continuum Model (CPCM) at all three stages [30]. The orbital plots provided in the following use a contour threshold of 0.03 au.

2. Results and discussion

2.1. Electronic absorption and emission properties

The absorption spectra of the complexes were recorded in acetonitrile (Fig. 1). The spectroscopic data are summarized in Table 1. The absorption spectra of these complexes are typical of the ruthenium polypyridyl complexes with intense UV absorption bands around 300 nm, assigned to ligand-centred π–π^* transitions and a broad band in the visible region around 450 nm attributed to the classical spin allowed metal-to-ligand charge-transfer (^{1}MLCT) transition. These assignments are confirmed by an analysis of the topology of the orbitals implied in the major TD-DFT transitions. The wavelength of the maximum absorbance of the ^{1}MLCT is relatively constant within this series of complex and agrees well with that reported with the unsubstituted homoleptic [Ru(bpy)$_3$]$^{2+}$ [10].

Excitation into the MLCT absorption band led to room temperature photoluminescence for all complexes in acetonitrile (Table 1). To determine the energy level of the triplet metal-to-ligand charge-transfer transition (^{3}MLCT) the emission spectra were also recorded at 77 K in a mixture of methanol/ethanol (4/1). As usual, the max-
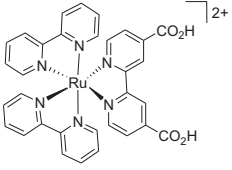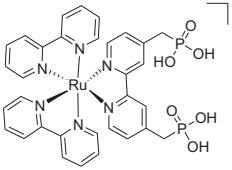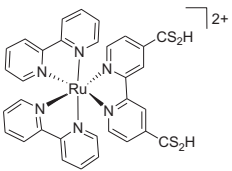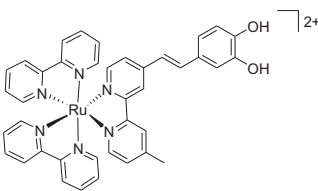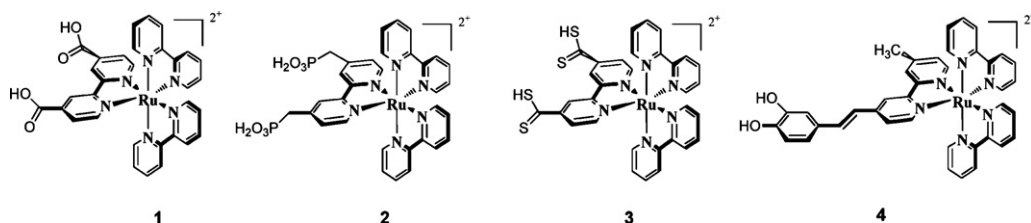

Fig. 1. Overlay of the absorption spectra of the complexes 1–4 recorded in acetonitrile.

Table 1
Spectroscopic data of the complexes **1–4** recorded in acetonitrile.

Sensitizer	λ_{max} ($\varepsilon \times 10^{-4}$) (nm/M^{-1} cm^{-1})	λ_{em} at RT (nm)	λ_{em} at 77 K^a (nm)	$E_{00}{}^b$ (eV)
1	474 (1.50) 288 (7.15)	685	628	1.97
2	450 (1.60) 288 (8.62)	632	587	2.11
3	457 (1.31) 288 (5.45)	684	600	2.08
4	456 (1.55) 286 (7.45)	653	597	2.08

[a] Recorded in frozen matrix (methanol/ethanol 4:1).
[b] Energy level of the triplet MLCT calculated from the maximum emission band in the spectrum at 77 K with the equation: $E_{00} = 1240/\lambda_{em}$.

imum emission is blue-shifted compared to the emission at room temperature (RT) owing to the absence of reorganization of the solvent sphere upon the intramolecular charge redistribution, which is typical of charge transfer excited-states. However, the energy level of the ^{3}MLCT in all complexes (with the exception of **2**) is decreased compared to that of [Ru(bpy)$_3$]$^{2+}$ (2.1 eV) indicating that the relevant orbital are modified by the anchoring groups (see electrochemistry and TD-DFT calculations). Energy wise, complex **2** is very similar to [Ru(bpy)$_3$]$^{2+}$, probably because of the isolating methylene spacers between the anchoring phosphonate groups and the chelating bpy.

2.2. Electrochemistry

The electrochemical properties of the sensitizers were explored by cyclic voltammetry in order to calculate the driving force for the hole injection reaction ($S^* \rightarrow S^- +$ hole/NiO$_{VB}$all valuable) and the regeneration reaction of the reduced sensitizer by the redox mediator ($S^- + 2/3\ I_3{}^- \rightarrow I_2{}^{\cdot-}$). The anchoring groups in complexes **1–4** have an intrinsic affinity for the electrode surfaces. As a result, voltammograms displayed strong adsorption/desorption features in particular in the cathodic range, as well as proton coupled redox processes, regardless of the working electrode material (platinum or amorphous carbon). Nevertheless, all complexes exhibited one reversible Ru(II)/Ru(III) oxidation wave at positive potentials and the expected reversible, ligand-based reduction waves in the cathodic region.

The increase of the metal based Ru(II)/Ru(III) oxidation potential in complexes **1** and **3**, compared to reference complex [Ru(bpy)$_3$]$^{2+}$(E_{Ox} = 1.26 V) indicates a decrease of the electron den-

sity on the metal and reflects the electron withdrawing character of the carboxylic and carbodithioic acid anchoring groups. Conversely, in complexes **2** and **4** the methyl phosphonic acid and the catechol groups are rather electron donating as witnessed by the cathodic shift of the oxidation potential. In the cathodic region, the reduction of the bipyridine occurs at an anodic potential relative to that of [Ru(bpy)$_3$]$^{2+}$ (E_{Red} = −1.35 V) when substituted with anchoring groups that stabilize the LUMO orbital by electron withdrawing or mesomeric effects (CO$_2$H for **1**, CS$_2$H for **3** and catechol for **4**), while it is cathodically shifted for methyl phosphonic substituents (**2**). Although sulphur is a rather electron rich element compared to oxygen, the carbodithioic acid groups stabilize the LUMO orbitals of the bipyridine by ca 0.2 eV relative to the unsubtituted bipyridine, evidencing thus a modest but significant stabilization by higher mesomeric effect than with oxygen (see DFT calculations).

These electrochemical data along with the energy level of the ^{3}MLCT enable to determine the Gibbs free energies (in eV) for the hole injection (ΔG_{inj} Eq. (2)), and regeneration (ΔG_{reg}, Eq. (3)) reactions:

$$\Delta G_{inj} = e \left[E_{VB}(NiO) - \left(E_{00}(S^*) + E \left(\frac{S}{S^-} \right) \right) \right], \tag{2}$$

$$\Delta G_{reg} = e \left[E \left(\frac{I_3^-}{I_2^{\cdot-}} \right) - E \left(\frac{S}{S^-} \right) \right], \tag{3}$$

where E_{VB}(NiO) is the valence band potential of nickel oxide (0.3 V vs SCE [31]), $E_{00}(S^*)$ is the energy of the ^{3}MLCT of the ruthenium sensitizer and $E(S/S^-)$ is its reduction potential. The calculated driving forces for both reactions are all negative. Except for complex **2** for which ΔG_{inj} is modest (ΔG_{inj} = −0.27 eV), for all the other complexes the Gibbs free energies are relatively large in absolute

Table 2
Electrochemical data and Gibbs free energies for the hole injection and regeneration reactions. The electrochemical study was carried out in dry DMF solution with Bu_4NPF_6 as supporting electrolyte and all the potentials are referenced relative to the saturated calomel electrode (SCE).

Dye	E_{red1}	E_{ox1}	E_{ox} Ru(II/III)	ΔG_{inj} (eV)	ΔG_{reg} (eV)
Ru(bpy)$_3$	−1.35		1.26		
1	−0.96		1.38	−0.54	−0.90
2	−1.41		1.24	−0.27	−0.89
3	−1.10	1.07[a] carbo dithioc	1.33	−0.57	−0.85
4	−1.23	1.28 catechols	1.28	−0.42	−0.71

[a] Irreversible process.

value, implying that the thermodynamic should not be the main limitation for the transfer processes (Table 2).

2.3. Surface binding experiments

An important property for a viable dye in DSSC is its strong attachment to the semiconductor surface as it governs the stability of the binding and the electronic coupling with the semiconductor. Indeed, the semiconductor-bound sensitizers should withstand prolonged exposure to electrolyte solutions without desorption and the dye excited-state should electronically communicate with the electronic level of the semiconductor to guaranty an efficient interfacial charge injection. The affinity of the binding groups in the complexes **1–4** was assessed by the determination of the association constant with NiO by recording the Langmuir adsorption isotherm in acetonitrile [32]. The gathered data were plotted using Langmuir formalism, and gave a straight line indicating that all the complexes follow the Langmuir adsorption model and therefore the self-assembly of the dye leads to a monolayer coverage of the NiO surface, at least, within the range of concentrations typically used for complexes adsorption onto semi-conductor surfaces (ca. 0.1–1 mM). Table 3 lists the values of the binding constants as well as the surface concentration at monolayer full coverage (Γ_{max}). The strongest affinity was obtained for the carboxylic acid group with a binding constant of 1.8×10^5 M^{-1}, which is higher than that reported for TiO$_2$ ($\sim 10^4$ M^{-1}) [17,32]. Although lower, the other binding groups display significant affinity towards nickel oxide demonstrating that they can effectively be used as anchoring groups to graft a sensitizer on NiO films. The binding constants are rank in the following order: CO$_2$H > PO$_3$H$_2$ > catechol > CS$_2$H, evidencing the lower affinity of the carbodithioic anchoring group for NiO. The surface concentrations at monolayer coverage (Γ_{max}) is another valuable piece of information extracted from the Langmuir isotherms, because the larger this value, the larger the absorbance of the NiO film and the smaller the naked NiO surface. The latter point is particularly important because it governs the recombination losses by dark current, which corresponds to the interception of the injected hole in NiO with the electrolyte (iodide). Interestingly, the surface coverage is not proportional to the binding constant, although we can reasonably assume that the projected surface of all complexes must be relatively similar to one another within **1–4**. The molar coverage is probably related to the overall charge of the complex, which depends on the anchoring group acidity, since its deprotonation will inevitably change the charge of the complex. The mean distance between

each complex on the surface is therefore controlled by its charge owing to the electrostatic repulsions. The surface coverage is indeed related to the pK$_a$ of the binding group since it follows the order PO$_3$H$_2$ > CO$_2$H ≈ CS$_2$H > catechol. We conclude that upon deprotonation such as with a phosphonic acid group, the overall charge of the complex decreases and a close packing of the dye on the NiO surface becomes more favourable.

2.4. TD-DFT results and molecular orbital analysis

The energy ranking (see Fig. 2) of the calculated LUMO orbitals qualitatively agrees with the reduction potentials measured by electrochemistry, since it follows the order CS$_2$H (-3.31 eV) > CO$_2$H (-2.89 eV) > catechol (-2.48 eV) > PO$_3$H$_2$ (-2.42 eV). This ordering follows the extension of the LUMO on the anchoring groups: small for CO$_2$H and catechol, null for PO$_3$H$_2$ but significant for CS$_2$H. The dithiocarboic acid group significantly stabilizes the LUMO of the bipy. This is the consequence of the delocalization, which is stronger with sulphur than with oxygen, owing to the larger size and lower electronegativity of the former.

TD-DFT simulations have been performed to determine the molecular orbitals implied in the main electronic transitions. The six frontier orbitals are collated in Fig. 3 for the four investigated compounds. Before analyzing the TD-DFT results, let us recall that the MLCT excited-state can be likened to a state in which an electron has been injected in a π* orbital, generally on a bpy ligand (virtual orbital), and a hole on the ruthenium centre (occupied orbital). Accordingly, for a hole injection probability from the sensitizer excited-state into the valence band of NiO, an optimal effect is reached when the relevant occupied orbital of the dye significantly extends on the anchoring groups in order to mix with the valence band wave function of the semiconductor. The degree of mixing can be estimated to a first extent from the size of the molecular orbitals on the binding groups. Conversely, the back charge recombination reaction, which was reported to be relatively fast in NiO DSSCs [33–37], will be slow if the electron (on the reduced dye) lies far away from the hole, which is localized in the semiconductor [23,33,38]. This condition is respected when the implied virtual orbitals (typically the LUMO) are remote from the anchoring groups.

Table 3
Binding constant (K) of the sensitizer to NiO surface and surface concentration at full monolayer coverage (Γ_{max}).
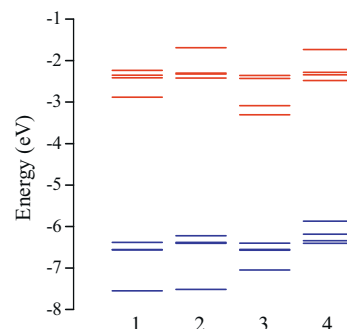
Complex	K (M^{-1})	Γ_{max} (μmol m^{-2})
1	1.8×10^5	0.89
2	1.7×10^4	1.2
3	3.8×10^3	0.78
4	4.9×10^3	0.53

Fig. 2. Orbital energy diagram (from HOMO-3 to LUMO + 3) for the four dyes.
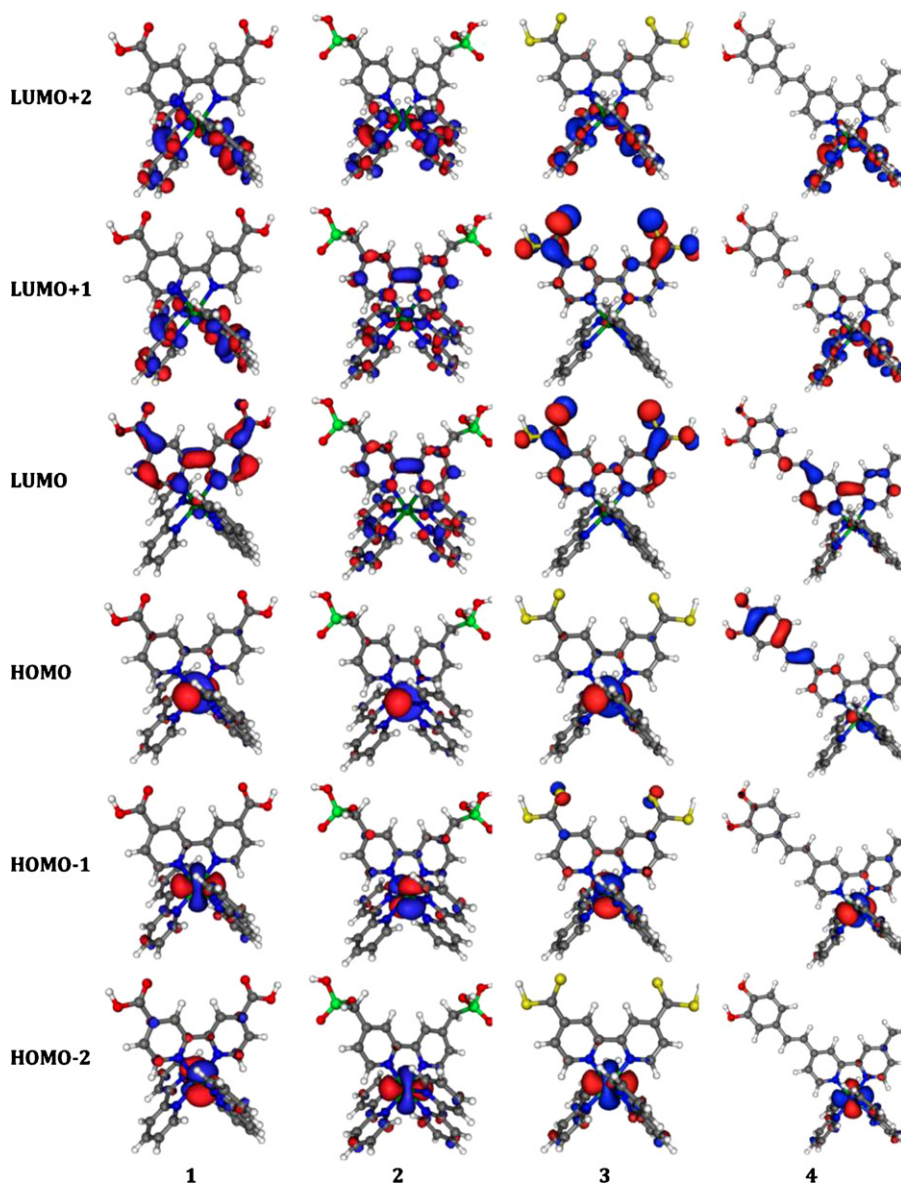
Fig. 3. Representations of the topology of the molecular orbitals (from HOMO-2 at the bottom to LUMO + 2 at the top) in the series of the ruthenium the complexes **1–4**.

TD-DFT calculations revealed more than one significant singlet transition in the visible domain for all compounds, e.g. 441 nm (f = 0.15), 391 nm (f = 0.14) and 383 nm (f = 0.10) for **1**. This outcome is consistent with the large bandwidth observed experimentally (see Fig. 1). Each transition mixes several molecular orbitals. Though a complete analysis of each peak is beyond the scope of the present work, this hints that the simple HOMO-LUMO approximation does not contain all the valuable information. Inspection of the localization of the frontier orbitals plotted in Fig. 3 reveals that for most complexes the three highest-lying occupied orbitals are centred on the ruthenium, whereas the virtual ones are π^* orbitals centred on the bipyridines, the LUMO being often on anchoring bpy, that is all four dyes share common patterns. However, this crude analysis should be refined. Indeed, in complexes **1** and **3**, the three virtual orbitals are almost purely Ru-based orbitals, whereas for **4**, the HOMO is relatively delocalized from the ruthenium d-π orbitals to the catechol binding group, implying that the electronic coupling with the semiconductor should be relatively stronger than for the other groups. The HOMO orbital dominates significantly the contribution of the T_1 state, but represents only 31% of the occupied orbitals implied in the visible (singlet) electronic transition. For the same dye **4**, the LUMO dominates the response of the two most intense visible bands as well as the first triplet state. As the LUMO of **4** is relatively close to the surface, **4** undergoes both positive (due to the HOMO's shape) and negative (due to LUMO's topology and weight) effects. In complex **2**, the LUMO, LUMO + 1 and LUMO + 2 display a significant contribution on the ancillary bipyridines. As each of these three orbitals represents (at least) 25% of the total TD-DFT contribution in the visible absorption band of **2**, and, as the first triplet state is dominated by LUMO and LUMO + 1 components, one predicts an advantage for this dye, as the captured electron would be located further away from the surface. For **1** and **3**, T_1 is dominated by the usual HOMO-LUMO promotion which is not optimal in the present case. Nevertheless, let us underline that in all the complexes **1–4** the energy spacing between the LUMO on the anchoring bpy and the higher lying LUMO on the ancillary bpy does not prevent electron hopping between the three ligands and therefore the electron is propably not fully localized on a specific bpy.

Table 4
Photovoltaic characteristics of the ruthenium sensitizers **1–4** recorded under AM 1.5 (100 mW cm^{-2}).

Dye	V_{oc} (mV)	J_{sc} (mA cm^{-2})	ff (%)	η (%)	$\Gamma_{max} \times \varepsilon \times 10^3$ (u.a.)
1	85	0.63	34	0.019	12.5
2	95	0.78	34	0.025	19.2
3	75	0.25	34	0.0065	10.2
4	85	0.65	32	0.018	8.2
C343	95	0.87	36	0.030	

In conclusion, these theoretical calculations revealed that no single compound simultaneously presents the ideal characteristics, i.e. an absorption implying an electronic promotion from an orbital delocalized on the anchoring group to an orbital located on the ancillary bpy far from the surface. Therefore, there must not be a large difference in the rate of charge recombination reaction. Concerning the magnitude of the electronic coupling from the ^{3}MLCT excited-state to the semiconductor wave function, it must be quite alike for the complexes **1–3**, but it is most probably larger with complex **4** substituted with catechol due to the shape of the HOMO.

2.5. Photovoltaic measurements

Sandwich-type solar cells were assembled using **1–4** sensitized nanocrystalline NiO as the working electrodes, platinized conducting glass as the counter electrode and iodide/triiodide in acetonitrile as electrolyte. The photovoltaic performances of solar cells based on these ruthenium complexes **1–4** and coumarine **C343**, as benchmark reference sensitizer, are summarized in Table 4. Fig. 4 shows the current–voltage characteristics of the dyes under AM 1.5 and in the dark (Fig. S3).

Clearly, all the complexes **1–4** display similar V_{OC} and ff values and therefore the overall photoconversion efficiencies η essentially differ by the value of J_{SC} which reflects differences in the incident photon to current conversion efficiency (IPCE). IPCE can be expressed as the product of the light harvesting efficiency [LHE(λ)] for photons of wavelength λ, the quantum yield of electron injection (Φ_{inj}) from the excited dye sensitizer to the valence band of the NiO electrode and the efficiency of collection of the injected electron (η_{coll}) in the external circuit:

$$\text{IPCE}(\lambda) = \text{LHE}(\lambda) \times \Phi_{inj} \times \eta_{coll} \tag{4}$$

In a first approximation, we can assume that Φ_{inj} is probably similar and high (close to unity) for the complexes **1–2** and **4**, because the injection driving force is relatively large (Table 2) and the ^{3}MLCT excited-state of ruthenium trisbipyridine complexes is particularly long-lived (hundreds of ns), while the hole injection in NiO is generally reported to be very fast (ps time scale) [23,33–37]. However, for complex **3** substituted with carbodithioic acid, the low photocurrent can be due to incomplete charge injection because ΔG_{inj} is modest (Table 2).

η_{coll} essentially depends on two charge recombination reactions. The first corresponds to the charge recombination between the reduced sensitizer and the hole in the VB of NiO and the second is the reaction of iodide with the injected hole on NiO or on FTO surface before it passes into the external circuit. The charge recombination between the reduced sensitizer and the hole in the VB of NiO is known to be generally very fast in NiO DSSCs and heavily depends on the distance between the two charges [23,33,38]. In ruthenium polypyridine complexes, it is well accepted that upon reduction the electron resides on the ligand featuring the lowest LUMO. Herein, the mean distance between the hole in NiO and the electron on the ruthenium complex must be quite alike, which indicates that the charge back recombination rate must be quite similar. As far as the reaction of iodide electrolyte with the injected hole on NiO is concerned, the series of complexes exhibit similar behaviour as the dark current characteristics (Fig. S3). Complex **4**, substituted by the catechol exhibits a slightly higher dark than the others, because the stiryl moiety certainly induces a different molecular packing on the NiO surface, which is indeed reflected by a lower surface coverage (Table 3). We therefore conclude that dark current recombination is not the main factor ruling the relative efficiencies of these complexes.

The last key parameter controlling the IPCE is therefore the light harvesting efficiency (LHE), explaining the differences in J_{SC}. Owing to the low extinction coefficient of the ruthenium complexes and to the systematic grey colour of the NiO electrode, it was impossible to record reliable absorption spectra of the stained NiO films. However, LHE is directly related to the extinction coefficient of the dye and the amount of adsorbed dyes on the NiO surface. Therefore, the product of Γ_{max} with ε(MLCT) must give a fair approximation of the relative LHE of these dyes, since these four ruthenium complexes **1–4** exhibit absorption spectra of similar shape (Fig. 1). Except for complex **3**, there is indeed a good correlation between these values which underscores that the photovoltaic
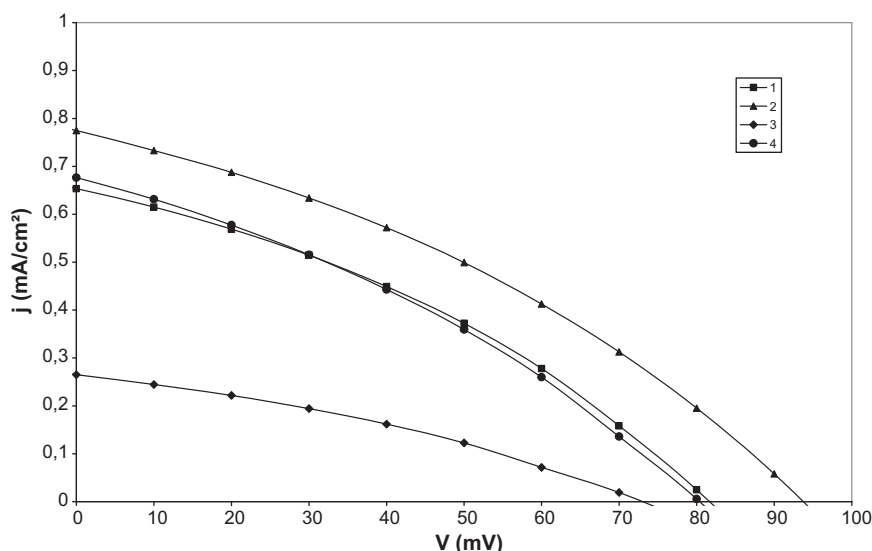
Fig. 4. Current–voltage characteristics of the complexes **1–4** recorded under AM 1.5.

efficiency differences within this series of complexes is essentially due to LHE differences (Table 2). This infers that the main reason at the origin of the relative efficiencies within complexes complexes **1–2** and **4** is due to differences in light collection efficiency, while complex **3** probably suffers from a lower hole injection quantum yield.

3. Conclusions

In this study, we prepared four trisbipyridine ruthenium complexes substituted by different anchoring groups and they were tested as sensitizers in NiO-based p-type dye-sensitized solar cells. We found that carboxylic acid displays the highest affinity for NiO surface, but it could be certainly advantageously replaced by a methyl phosphonic acid or catechol moieties, which also significantly bind to NiO surface. Methyl phosphonic acid is a valuable anchoring group to prepare stable linkage with a metal oxide, as confirmed with sensitizers for classical TiO_2 DSSC [12–14,17], while catechol is most certainly another promising anchoring group to enhance the electronic coupling with the semiconductor (mixing of the HOMO of the sensitizer with the wave function of the valence band of NiO) because it is electron richer than the classical carboxylic acid. We also showed that some of these very simple ruthenium complexes exhibit photoconversion efficiencies in the same range as that of the classical benchmark reference coumarin **C343**, indicating that much higher performances could certainly be obtained with this family of complexes if one follows the molecular engineering rules presented below. Indeed, the photovoltaic performances of these MLCT excited state polypyridine metal complexes (with Ru^{II}, Os^{II}, Ir^{III} and probably Cu^{I}) could be certainly enhanced by first preparing neutral heteroleptic complexes such as the very famous and highly performing cis-bis(thiocyanato)bis-(2,2′-bipyridine-4,4′-dicarboxylic acid) ruthenium(II) sensitizer used in TiO_2 based DSSCs [39]. This will prevent the electrostatic repulsions observed with charged dyes and favour close molecular packing on the NiO surface. Secondly, by using ancillary ligands exhibiting much stronger π-accepting properties than the ligand functionalized by the anchoring groups, the absorption spectrum would be shifted towards lower energies and enhance the transition dipolar moment hence the extinction coefficient [40]. This feature would also move away the electron on the reduced dye from the NiO surface upon hole injection and slow down the charge recombination. To reach these goals, methyl phosphonic acid and particularly catechol represent particularly suitable anchoring groups, because they enable to polarize the charge shift in the sensitizer in a more appropriate direction to favour the hole injection in the p-SC and to shift the negative electronic density away from the surface. These results open the way towards the design of new and more efficient transition metal complexes for p-DSSC and this goal is under way in our laboratory.

Acknowledgements

Appendix A. Supplementary data

Supplementary data associated with this article can be found, in the online version, at doi:10.1016/j.jphotochem.2011.02.025.

References

[1] F. Odobel, L. Le Pleux, Y. Pellegrin, E. Blart, Acc. Chem. Res. 43 (2010) 1063.
[2] R. Jose, A. Kumar, V. Thavasi, K. Fujihara, S. Uchida, S. Ramakrishna, Appl. Phys. Lett. 93 (2008) 023125.
[3] F. Aiga, T. Tada, J. Mol. Struct. 658 (2003) 25.
[4] M. Nilsing, P. Persson, L. Ojamaee, Chem. Phys. Lett. 415 (2005) 375.
[5] L. Gundlach, R. Ernstorfer, F. Willig, Prog. Surf. Sci. 82 (2007) 355.
[6] A.S. Polo, M.K. Itokazu, N.Y. Murakami Iha, Coord. Chem. Rev. 248 (2004) 1343.
[7] K. Kalyanasundaram, M. Grätzel, Coord. Chem. Rev. 177 (1998) 347.
[8] R. Argazzi, N.Y. Murakami Iha, H. Zabri, F. Odobel, C.A. Bignozzi, Coord. Chem. Rev. 248 (2004) 1299.
[9] V. Balzani, F. Scandola (Eds.), Supramolecular Photochemistry, Reidel, Chischester, UK, 1991.
[10] S. Campagna, F. Puntoriero, F. Nastasi, G. Bergamini, V. Balzani, Top. Curr. Chem. 280 (2007) 117.
[11] W.J. Youngblood, S.-H.A. Lee, Y. Kobayashi, E.A. Hernandez-Pagan, P.G. Hoertz, T.A. Moore, A.L. Moore, D. Gust, T.E. Mallouk, J. Am. Chem. Soc. 131 (2009) 926.
[12] J.J. Concepcion, J.W. Jurss, M.K. Brennaman, P.G. Hoertz, A.O.T. Patrocinio, N.Y. Murakami Iha, J.L. Templeton, T.J. Meyer, Acc. Chem. Res. 42 (2009) 1954.
[13] S. Caramori, V. Cristino, R. Argazzi, L. Meda, C.A. Bignozzi, Inorg. Chem. 49 (2010) 3320.
[14] E. Bae, W. Choi, J. Phys. Chem. B 110 (2006) 14792.
[15] T. Nann, S.K. Ibrahim, P.-M. Woi, S. Xu, J. Ziegler, C. Pickett, Angew. Chem. Int. Ed. 49 (2010) 1574.
[16] K. Kils, E.I. Mayo, B.S. Brunschwig, H.B. Gray, N.S. Lewis, J.R. Winkler, J. Phys. Chem. B 108 (2004) 15640.
[17] I. Gillaizeau-Gauthier, F. Odobel, M. Alebbi, R. Argazzi, E. Costa, C.A. Bignozzi, P. Qu, G.J. Meyer, Inorg. Chem. 40 (2001) 6073.
[18] G. Sprintschnik, H.W. Sprintschnik, P.P. Kirsch, D.G. Whitten, J. Am. Chem. Soc. 99 (1977) 4947.
[19] A.D. Shukla, B. Whittle, H.C. Bajaj, A. Das, M.D. Ward, Inorg. Chim. Acta 285 (1999) 89.
[20] R.M. Leasure, W. Ou, J.A. Moss, R.W. Linton, T.J. Meyer, Chem. Mater. 8 (1996) 264.
[21] J.E. Collins, J.J.S. Lamba, J.C. Love, J.E. McAlvin, C. Ng, B.P. Peters, X. Wu, C.L. Fraser, Inorg. Chem. 38 (1999) 2020.
[22] S. Sumikura, S. Mori, S. Shimizu, H. Usami, E. Suzuki, J. Photochem. Photobiol., A 199 (2008) 1.
[23] A. Nattestad, A.J. Mozer, M.K.R. Fischer, Y.B. Cheng, A. Mishra, P. Baeuerle, U. Bach, Nat. Mater. 9 (2010) 31.
[24] M.J. Frisch, G.W. Trucks, H.B. Schlegel, G.E. Scuseria, M.A. Robb, J.R. Cheeseman, G. Scalmani, V. Barone, B. Mennucci, G.A. Petersson, H. Nakatsuji, M. Caricato, X. Li, H.P. Hratchian, A.F. Izmaylov, J. Bloino, G. Zheng, J.L. Sonnenberg, M. Hada, M. Ehara, K. Toyota, R. Fukuda, J. Hasegawa, M. Ishida, T. Nakajima, Y. Honda, O. Kitao, H. Nakai, T. Vreven, J.A. Montgomery Jr., J.E. Peralta, F. Ogliaro, M. Bearpark, J.J. Heyd, E. Brothers, K.N. Kudin, V.N. Staroverov, R. Kobayashi, J. Normand, K. Raghavachari, A. Rendell, J.C. Burant, S.S. Iyengar, J. Tomasi, M. Cossi, N. Rega, J.M. Millam, M. Klene, J.E. Knox, J.B. Cross, V. Bakken, C. Adamo, J. Jaramillo, R. Gomperts, R.E. Stratmann, O. Yazyev, A.J. Austin, R. Cammi, C. Pomelli, J.W. Ochter- ski, R.L. Martin, K. Morokuma, V.G. Zakrzewski, G.A. Voth, P. Salvador, J.J. Dannenberg, S. Dapprich, A.D. Daniels, O. Farkas, J.B. Foresman, J.V. Ortiz, J. Cioslowski, D.J. Fox, Gaussian 09 Revision A. 02, Gaussian Inc, Wallingford CT, 2009.
[25] D. Jacquemin, E.A. Perpète, I. Ciofini, C. Adamo, Acc. Chem. Res. 42 (2009) 326.
[26] C. Adamo, V. Barone, J. Chem. Phys. 110 (1999) 6158.
[27] J.F. Guillemoles, V. Barone, L. Joubert, C. Adamo, J. Phys. Chem. A 106 (2002) 11354.
[28] T. Yanai, D.P. Tew, N.C. Handy, Chem. Phys. Lett. 393 (2004) 51.
[29] S. Fantacci, F. de Angelis, A. Selloni, J. Am. Chem. Soc. 125 (2003) 4381.
[30] J. Tomasi, B. Mennucci, R. Cammi, Chem. Rev. 105 (2005) 2999.
[31] J. He, H. Lindström, A. Hagfeldt, S.-E. Lindquist, J. Phys. Chem. B 103 (1999) 8940.
[32] A. Fillinger, B.A. Parkinson, J. Electrochem. Soc. 146 (1999) 4559.
[33] A. Morandeira, J. Fortage, T. Edvinsson, L. Le Pleux, E. Blart, G. Boschloo, A. Hagfeldt, L. Hammarström, F. Odobel, J. Phys. Chem. C 112 (2008) 1721.
[34] M. Borgström, E. Blart, G. Boschloo, E. Mukhtar, A. Hagfeldt, L. Hammarström, F. Odobel, J. Phys. Chem. B 109 (2005) 22928.
[35] A. Morandeira, G. Boschloo, A. Hagfeldt, L. Hammarström, J. Phys. Chem. B 109 (2005) 19403.
[36] A. Morandeira, G. Boschloo, A. Hagfeldt, L. Hammarström, J. Phys. Chem. C 112 (2008) 9530.
[37] P. Qin, J. Wiberg, E.A. Gibson, M. Linder, L. Li, T. Brinck, A. Hagfeldt, B. Albinsson, L. Sun, J. Phys. Chem. C 114 (2010) 4738.
[38] E.A. Gibson, A.L. Smeigh, L.L. Pleux, J. Fortage, G. Boschloo, E. Blart, Y. Pellegrin, F. Odobel, A. Hagfeldt, L. Hammarström, Angew. Chem. Int. Ed. 48 (2009) 4402.
[39] B. O'Regan, M. Grätzel, Nature 353 (1991) 737.
[40] P.A. Anderson, G.F. Strouse, J.A. Treadway, F.R. Keene, T.J. Meyer, Inorg. Chem. 33 (1994) 3863.